Strain monitoring of cement-based materials with embedded polyvinyl alcohol - carbon nanotube (PVA-CNT) fibers

Zoi S. Metaxa
National Technical University of Athens, Laboratory of Strength and Materials, 9 Heroes Polytechnion Str., 15780 Athens, Greece

Wilfrid Neri, Philippe Poulin
University of Bordeaux, Centre de Recherche Paul Pascal – CNRS, Avenue Schweitzer, 33600 Pessac, France

Nikolaos D. Alexopoulos
University of the Aegean, Department of Financial Engineering, 821 00 Chios, Greece
nalexop@aegean.gr

ABSTRACT. This article investigates the possibility of exploiting innovative polyvinyl alcohol fibers reinforced with carbon nanotubes (PVA-CNT fiber) as a strain sensor in cement mortars used in the restoration of Cultural Heritage Monuments. Two types of PVA-CNT fibers were embedded in the matrix at a short distance from the bottom of the beam and their readings were correlated with traditional sensors, e.g. strain gauges and Fiber Optic Bragg Gratings. The Electrical Resistance Change (ERC) of the embedded PVA-CNT fiber was in-situ monitored during four-point bending mechanical tests. For the case of coated PVA-CNT fiber, a linear correlation of the applied strain at the bottom surface of the specimen along with ERC values of the fiber was noticed for the low strain regime. For the case of incremental increasing loading – unloading loops, the coated and annealed PVA-CNT fiber gave the best results either as embedded or as 'surface attached' sensor that exhibited linear correlation of ERC with applied strain for the low applied strain regime as well as hysteresis loops during unloading. The article discusses their high potential to be exploited as strain/damage sensor in applications of civil engineering as well as in restoration of Monuments of Cultural Heritage.

KEYWORDS. Cement-based materials; Sensing; FOBGs; Monitoring.

INTRODUCTION

The ad-hoc accurate and thorough knowledge of the mechanical behaviour of building materials used in the restoration of Cultural Heritage Monuments is fundamental for the protection of their structural integrity. However, most of the traditional techniques used in the laboratory and in the field, such as strain-gauges, dial-gauges, extensometers, and Linear Variable Differential Transformers (LVDTs), provide data drawn from the materials' external surface. Therefore, gathering information about the internal events, for example local failures and micro-fracture, which precede those detected on the materials' surface, is challenging. The technological need to mine data from the interior of the restored joints and specimens were reported by Kourkoulis et al [1]. In a series of articles, e.g. [2-4] the important role of the interphases of the connecting materials used in the interior of the restored joints are noted. Additionally, several researchers underlined the important aspects of straining of the connecting members of the joint that are well in the interior of the restored Monument of Cultural Heritage, e.g. [5-7]. To cope with this problem, innovative measuring techniques should be used in parallel with the traditional ones for calibrating purposes.

An already mature technique for damage monitoring of cement-based materials is the embedded glass fiber optical sensors. In the areas of local strain change, loss of the transmitted light signal [8] occurs that corresponds to damage within the monitoring region [9]. The detection can be performed with small embedded Bragg grating sensors with nominal diameter of approximate 120 µm, e.g. [10-12]. Nevertheless, this technique has several limitations, e.g. monitoring of the matrix transverse cracking. In addition, a dense network of optical fibers would be needed to fully monitor the complete structure that is economically not sustainable.

Acoustic emission is another technique to monitor damage development in cement-based materials. Initiation of damage mechanisms (tension or shear) induce different crack tip motions, resulting in quite different AE characteristics. These distinct acoustic events can therefore be directly linked to a specific type of failure or can be evaluated in a cumulative manner to characterize the state of damage of the matrix, e.g. [13, 14]. Despite the numerous articles in this scientific field, the provided AE data are usually not sufficient to solely characterize the structural health of the matrix and another technique is required to cross-plot the necessary information [15, 16].

In this study, the exploitation of different types of advanced fibers made from polyvinyl alcohol (PVA) reinforced with carbon nanotubes (CNTs) for sensing the mechanical performance of the cement mortar used for the restoration of Acropolis' Parthenon will be investigated. These new innovative PVA-CNT fibers have small dimensions (d = 40 to 60 µm) and exhibit excellent piezoresistive characteristics and ductility that exceeds 100 % elongation [17]. Manufacturing of the specific fibers can be done by a potentially scalable process already reported [18]. Previous research on epoxy resin composites reinforced with glass fibers showed that the aforementioned PVA-CNT microfibers can be successfully embedded in the composite [19] and can be used for strain/damage monitoring purposes of non-conductive composites under tensile and bending loading tests [20, 21].

EXPERIMENTAL PROCEDURE

Manufacturing of prismatic cement mortar specimens

White cement, Portland type, with the code name AALBORG WHITE and class CEM I 52,5R was used in the present study. The specific cement is manufactured from exceptional pure limestone and fine-grain quartz sand. The mineralogical phases of the white cement used as well as several characteristics of the cement can be seen in Tabs. 1 and 2, respectively. Two different sand types were used: (a) coarse grained quartz sand from 1 to 2 mm as well as (b) fine-grain quartz sand M32 with average grain size of 260 mm. The selection of the above materials has been performed according to several criteria, extensively discussed in [4].

C3S	C2S	C3A	C4AF
77 (wt%)	16 (wt%)	5 (wt%)	1 (wt%)

Table 1: Mineralogical phases of white cement.

In the present work, the following kinds of sensors were used: (a) 2 different types of CNT reinforced PVA fibers (PVA-CNT fibers). The first type will be called in the following as "coated PVA-CNT" fiber, while the second one as "coated and annealed PVA-CNT" fiber, that had different process parameters as discussed in the following. This kind of sensors

utilizes the electrical resistance change method for the damaged areas of the matrix. The second type of sensor used was (b) Fiber Optical Bragg Gratings (FOBG) in order to detect damage on the surrounding medium through the transmission of light within the fiber.

Density (kg/m³)	3130
Phenomenological density (kg/m³)	1100
Curing time of cement according EN 196-3	120 min

Table 2: Physical characteristics of white cement.

The PVA-CNT fibers were fabricated at the facilities of University of Bordeaux (CNRS-CRPP). Multi-wall carbon nanotubes (MWCNTs) with 98 % purity were used from Arkema, Lacq in Aquitaine province of France. Typical the fibers have a concentration of approximate 13 wt% MWCNTs. For specific applications, the manufactured fibers can be coated with MWCNTs in order to increase their surface conductivity [18]. In the present case, the coated PVA-CNT fibers had been coated with an immersion technique in an aqueous solution with dispersed MWCNTs. The solution contained 0.5 wt% MWCNTs and 0.7 wt% SDS; the latter is a common surfactant, widely used to stabilize MWCNTs in aqueous solutions. The fibers were dried before use and several images (macro photos as well as cross-sectional) can be seen in [19].

The coated and annealed PVA-CNT fibers were also coated fibers according to the already described procedure that had an additional heat treatment stage. The annealing of the polymer (approximately around 150 °C) well above the glass temperature transition (T_g) temperature, makes the polymer softer, thus enabling the more efficient attachment of the MWCNTs on the surface of the fiber. Additionally, it improves the crystallinity as well as the mechanical properties of the manufactured fibers.

Two types of cement-based prismatic specimens were manufactured: Type I specimen deals with sensors that were embedded during manufacturing. Type II deals with surface-attached sensors; they were attached on the specimens when the curing process of the cement-based specimens ended and just before mechanical testing.

The same mixing procedure was followed for all the cement-based specimens according to ASTM C305 [22]. Mixing was performed using a standard 5 l mixer made from TECHNOTEST®. Initially, cement and water were placed into the mixing bowl. Mixing started immediately at a slow speed of (140 ± 5 r/min) and lasted for 30 s. Following, both types of sand (course and fine), that were premixed, were slowly added to the paste over a 30 s period, while mixing at slow speed. Next, the materials were mixed for 30 s at medium speed (285 ± 10 r/min). The mixer was stopped for 90 s to let the mortar stand, during the first 30 s of this interval; any mortar that had collected on the side of the bowl was scraped down into the batch. To certify the homogeneity of the mortar, as a final step, the materials were mixed at medium speed for 90 s.

Figure 1: (a) Mold for the manufacturing of the prismatic specimens with already installed PVA-CNT fiber and specific oil and (b) casted mixture in the mold for two specimen's preparation.

Customized prismatic molds made from aluminum having a length of 80 mm and a cross-section of 20 mm × 20 mm, were used. Very thin holes of approximately 1 mm dimeter, suitable for the placement of PVA-CNT fibers / FOBGs, were drilled at both sides of the molds. Before casting, suitable concrete demolding oil was used to facilitate the specimens' removal. Then the fibers were placed in the molds as shown in Fig. 1a and casting was performed (Fig. 1b).

Immediately after casting, the specimens were covered with plastic wrap and were left to cure for 24 h at room temperature. After demolding, the saturated wet covering method was adopted for further curing of the samples. This was to make sure that specimens were kept in a wet condition during the curing period without damaging/affecting the fibers. The specimens were covered with wet cloths (water saturated with calcium hydroxide) and were sealed with plastic wrap.

According to Nahata et al. [23] mortars cured using the aforementioned procedure demonstrate a slightly lower compressive strength compared to specimens cured in water immersion (specimens cured in water tank at room temperature) demonstrating that the curing procedure adopted in this study does not compromise the mechanical performance of the material. At the age of 28 days the specimens with the embedded sensors were uncovered and were ready for mechanical testing (Fig. 2a and b), while for several specimens the sensor was externally attached (Fig. 2c) before testing.

Mechanical testing

For the execution of the mechanical tests, a number of experimental devices were used (Fig. 3) that will be explained in the following. An MTS Insight loading frame was used to record the changes in crosshead displacement and mechanical load, a multimeter for the electrical resistance of the embedded PVA-CNT fiber, an interrogator for the respective measurements of the FOBG sensor and finally a data logger for the measurements of the strain gauges.
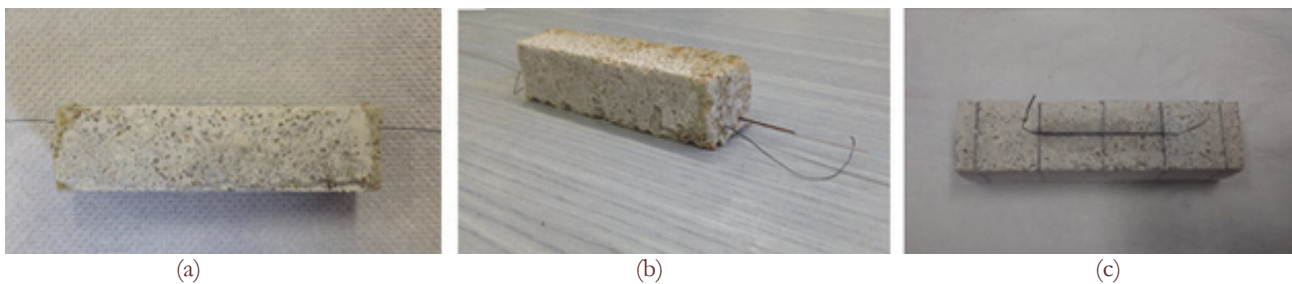

| | | |
| (a) | (b) | (c) |

Figure 2: (a) Prismatic specimen with embedded PVA – CNT fiber (Type I), (b) specimen with embedded PVA – CNT fiber and FOBG fiber and (c) specimen with externally attached PVA – CNT fiber (Type II).
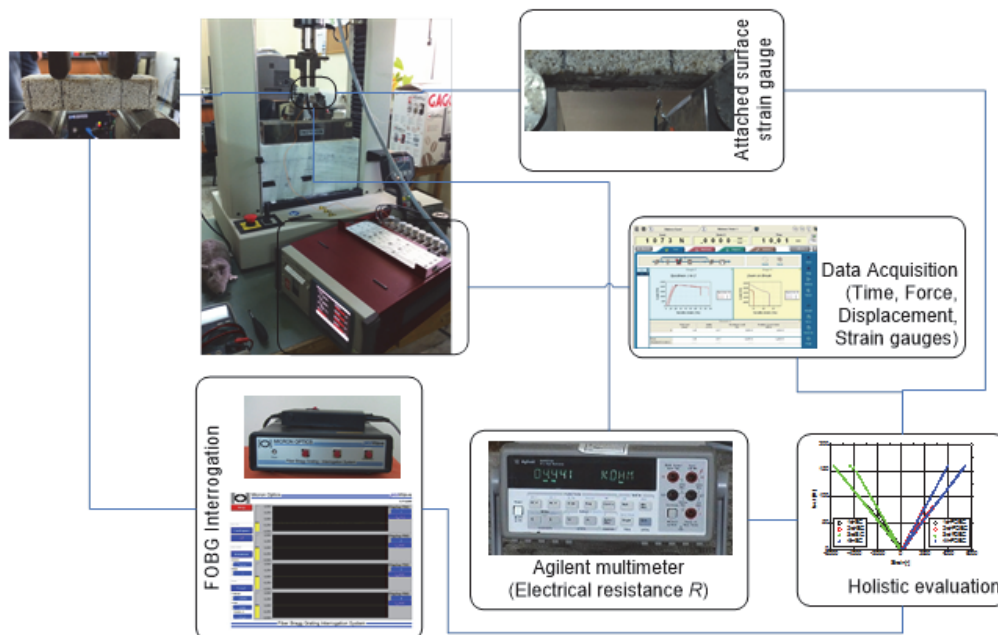

Figure 3: Flow diagram of the experimental procedure.

Two types of prismatic specimens were evaluated. The first one (Type I) has embedded sensors and the second one (Type II) has surface attached sensors. The geometrical dimensions of all specimens can be seen in Fig. 4a (Type I specimen is shown), while the loading supports (four point bending) can be seen in Fig. 4b. The three-point bending tests had been performed on specimens with embedded PVA-CNT fiber on the tensile region (fiber close on bottom surface of the specimen). The correctly adjusted / placed specimen at the jigs of the testing machine can be seen in Fig. 5a, where surface-attached strain gauges were also used to monitor the strain changes at the bottom surface of the prismatic specimens (Fig. 5b). As the incremental loading steps have been made to specific levels of fracture stress of the material,

the testing machine was load-controlled with a crosshead speed of 0.1 mm/min. Evaluation of the four point bending (4pb) mechanical tests have been performed according to ASTM D6272 [24]. During testing, crosshead displacement, load and the strain gauges measurements were continuously recorded and stored in a P/C.

An Agilent multimeter was used to record in situ the electrical resistance data of the specimen's embedded PVA-CNT fiber during mechanical loading. A DC voltage of 10 V was applied to cables connected to the PVA-CNT fiber of the specimens (Fig. 3), the current was measured and the resistance was calculated from these values. The resistance measurements were performed in a two-point measurement set-up in the longitudinal direction. Data acquisition of 1 Hz was also used for the resistance measurements and stored simultaneously in the P/C of the testing machine. Electrical resistance change (ERC) values were post-calculated form the initial resistance values.

The optical fiber sensors used were Bragg gratings of 2 mm nominal length. The reflectivity of these sensors was of the order of 20 %, in order to ensure adequate spectrum reflection and at least 50 cm of free optical fiber should be available at each side for adaptation of connectors. Selected center wavelength was 1540 ± 1 nm, while Δλ was approximate ~ 0.7 nm. An interrogation system was used to measure the wavelength changes due to the mechanical field loading and evaluate the equivalent strain values. The wavelength data were afterwards converted to axial strains measured in the vicinity of the Bragg grating sensors, based on the fundamental equation for constant temperature for mechanically and optically isotropic optical fibers:

$$\Delta\lambda_{\mathrm{B}} = \lambda_{\mathrm{B}} \cdot \left(1 - \rho_a\right) \cdot \Delta\varepsilon + \lambda_{\mathrm{B}} \cdot \left(\alpha + \xi\right) \cdot \Delta T \tag{1}$$

that relates the wavelength changes to the axial strain of the fiber at the sensor area through the sensitivity coefficient λ_{B}. Term $\Delta\lambda_{\mathrm{B}}$ is the change in Bragg wavelength, ρ_a, a and ξ are respectively the photoelastic, thermal expansion and thermo-optic coefficients of the fibre, $\Delta\varepsilon$ is the strain and ΔT is the temperature change, respectively. In the present work, λ_{B} was measured via calibration and for the specific sensor it was found to be equal to 0.89 με / pm or inversely 1.12 pm / με. Using Eq. (1), all wavelength shifts were collected from the interrogator device and the respected axial strains were calculated.
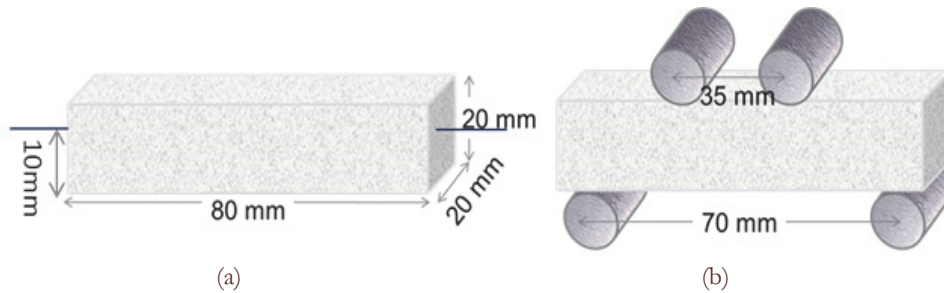

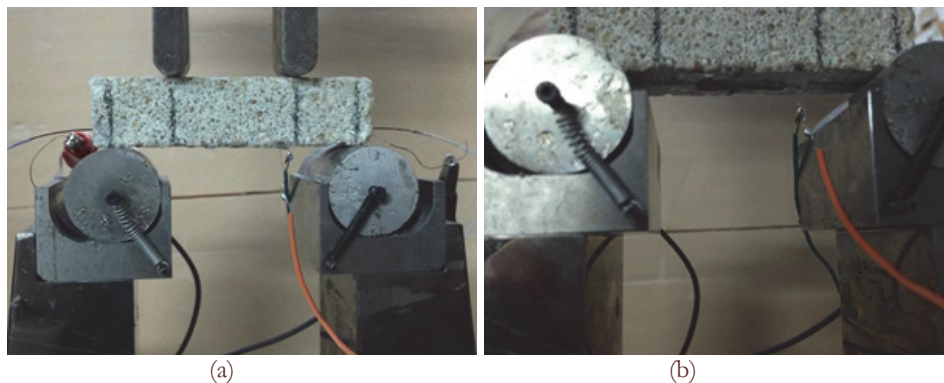Figure 4: Sketch of the (a) geometrical dimensions and (b) testing supports of the specimen.

Figure 5: (a) Installed specimen with embedded PVA-CNT fiber and (b) magnification of the bottom side of the specimen with surface attached strain gauge.

For the Type I specimens (with embedded sensors), the following tests have been performed: (a) monotonic loading till fracture and (b) incrementally increasing loadings - unloadings till fracture. For the Type II specimens (with attached

sensors) constant amplitude loadings - unloadings have been performed to assess the screening of the sensors. In total 11 different test categories were performed that can be seen in Tab. 3.

	Reference	Coated PVA-CNT fiber	Coated and annealed PVA-CNT fiber
(-)	P	-	-
Attached surface strain gauge	P	M, P	M, P
FOBG and attached surface strain gauge	M, P	P	P

NOMENCLATURE: M: Monotonic four point bending (4pb) till fracture
P: Progressive damage accumulation in 4pb (incremental loading-unloadings till fracture)

Table 3: List of the experimental tests.

RESULTS AND DISCUSSION

The experimental bending test results will be presented and discussed in this section in order to establish a useful correlation of the readings of the embedded / attached sensors with the mechanical deformation of the specimen.

Monotonic bending tests
Monotonic tests have been performed on different specimens for the three investigated embedded sensors, (a) coated PVA-CNT fiber, (b) coated and annealed PVA-CNT fiber and (c) FOBG. Fig. 6 shows the comparison of the mechanical response of the each specimen during four-point bending testing. The specimens with the embedded PVA-CNT fiber seem to resolve identical maximum stress values along with axial deformation at the bottom level of the specimen. All four different cases seem to have approximately the same mechanical response and the average fracture stress is around 3 MPa.
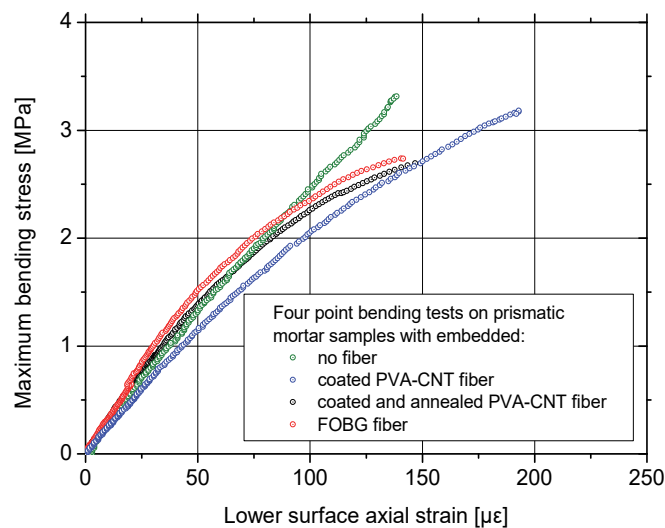

Figure 6: Comparison of the monotonic mechanical response of the specimens with embedded sensors.

Fig. 7 shows the mechanical response of the material along with the simultaneous electrical resistance response of the embedded PVA-CNT fiber for the monotonic loading of the specimen till the macroscopic fracture. Fig. 7a corresponds to the coated PVA-CNT fiber, while the respective results of the coated and annealed PVA-CNT fiber can be seen in Fig. 7b. By comparing the two diagrams, it can be clearly seen that linearity is evident in both types of fibers for the low applied loadings that corresponds to the elastic loading regime. This linearity is no longer evident with increasing the applied bending stresses. Additionally, for the case of the coated PVA-CNT fiber this linear stage ends at higher ERC values that allows for better screening of the results. This loss in linearity is probably due to the partial fracture of the

interphase between the embedded fiber and surrounding matrix [19] that gives a sudden drop in ERC values as the fiber is partially unloaded. This pattern of sudden drops in ERC values can be noticed for even higher stress level and can be additionally due to micro-cracking [20] that approximately starts at the 30 % of the maximum bending stress (around 1 MPa) and fracture for higher applied stresses.
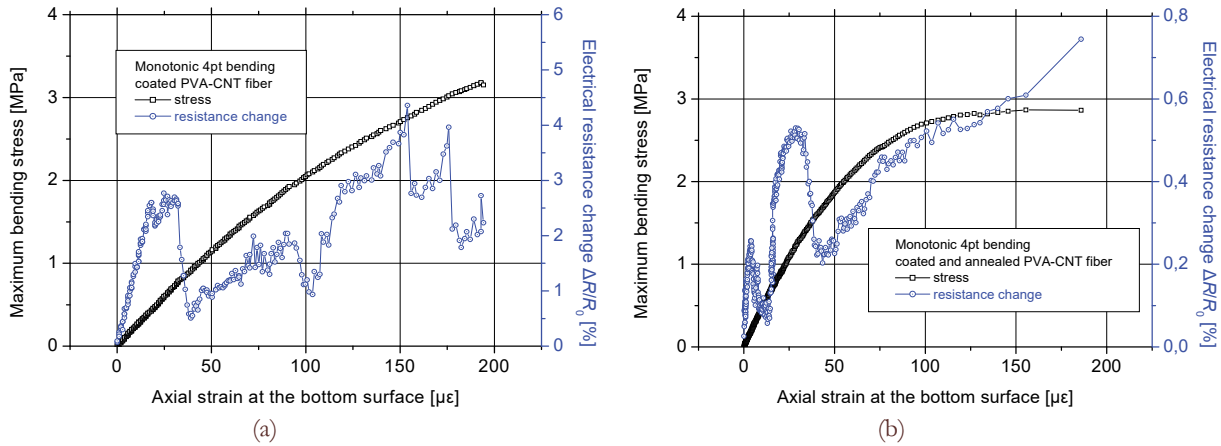

Figure 7: (a) Mechanical response of the prismatic specimens and electrical resistance response of the different embedded PVA-CNT fiber type (a) coated and (b) coated and annealed.

Constant amplitude loading - unloading loops
The test results for the constant amplitude tests will be described in this section. Ten (10) loading – unloading loops were performed with maximum bending load being 80 N that corresponds to approximately 0.5 MPa that is definitely within the elastic loading regime without the presence of micro-cracking. Fig. 8 shows the mechanical response of the type I specimen (stress in red color while strain in black color) as well as the ERC values of the embedded fiber (in blue color) over testing time. Despite the low maximum loading stress, residual strain values can be noticed after several cycles that can be attributed to developed damage inside the specimen. The strain loops seems to take low amplitude values; after the tenth loading loop strain amplitude goes from 1 to 2.5 % axial strain that is almost half when compared with the first loading loop. ERC values show increased scatter values that might be a problem of the high sampling frequency. The peak and valleys of the ERC values can be hardly distinguished in the diagram; however, the trend shows that ERC is continuously increasing with the constant amplitude loadings. Such a trend was also noticed for the case of monitoring glass fiber reinforced plastic with embedded PVA-CNT fiber and ERC was directly compared with the residual strain of the composites that is clearly evidence of induced damage in the matrix of the material [20]. This is obviously the case with the existing test results.
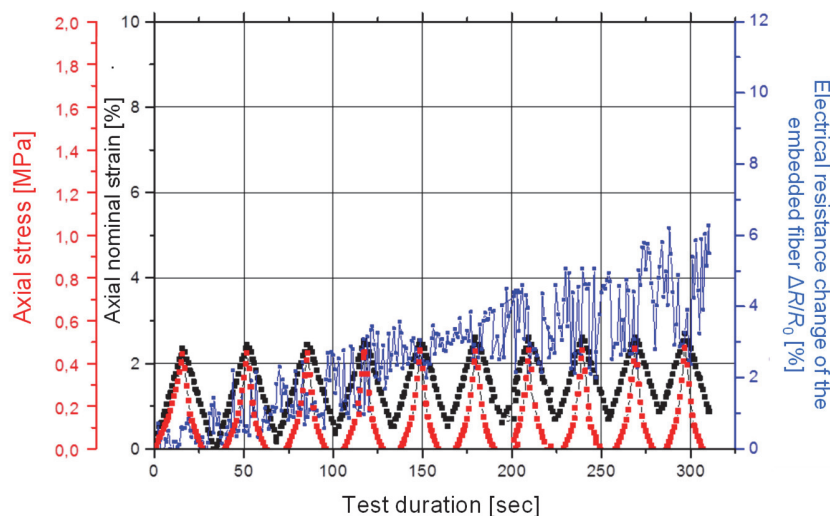

Figure 8: Mechanical response of the type I specimen with embedded coated PVA-CNT fiber under constant amplitude loading – unloading loops and electrical response of the embedded fiber.

Fig. 9 shows the respective test results for the type II specimen with the surface attached fiber. Strain measurements also show a small reduction on the amplitude after some test cycles; ERC measurements seems to be vague and definitely lower sampling rate should have been used. Though the surface-attached fiber gives readings during mechanical testing, optimization will be performed in the near future regarding the preparation of the surface, medium for the proper attachment of the fiber [19], as several vague recordings might be due to local loss of coherency of the interphase of the connecting medium (glue) with the substrate and therefore loading transfer of the specimen to the sensor is not optimal.
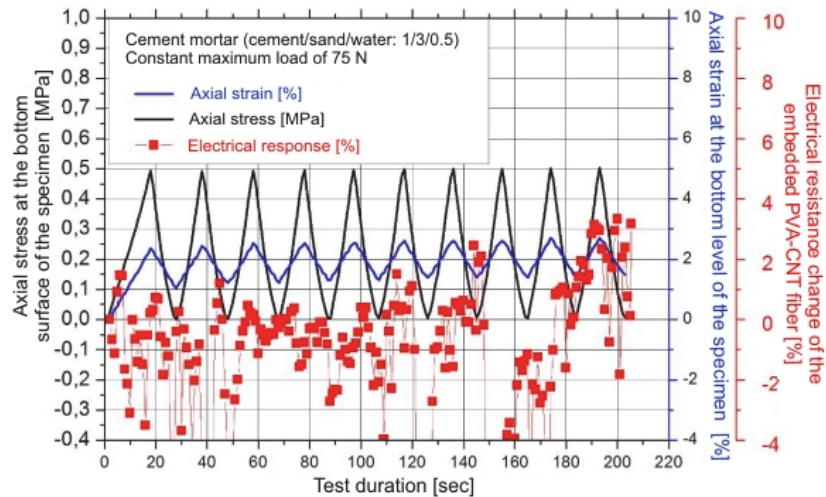

Figure 9: Mechanical response of the Type II specimen with surface attached coated PVA-CNT fiber under constant amplitude loading – unloading loops and electrical response of the attached fiber.

Incrementally increasing loading - unloading loops

In this section the test results of continuous increasing loading – unloading loops will be reported. Tests were performed with continuous increasing maximum load of 40 N after every unloading and hereafter will be called as progressive damage accumulation tests. Typical applied bending force protocol over testing time can be seen in Fig. 10a, while Fig. 10b shows the typical mechanical response (stress-strain) of a specimen for the fourteen cycles till fracture. Residual strain values are noticed every single unloading and the higher the loading value is, the higher the residual axial strain is. Additionally, hysteresis loops are evident for the latest loading cycles.
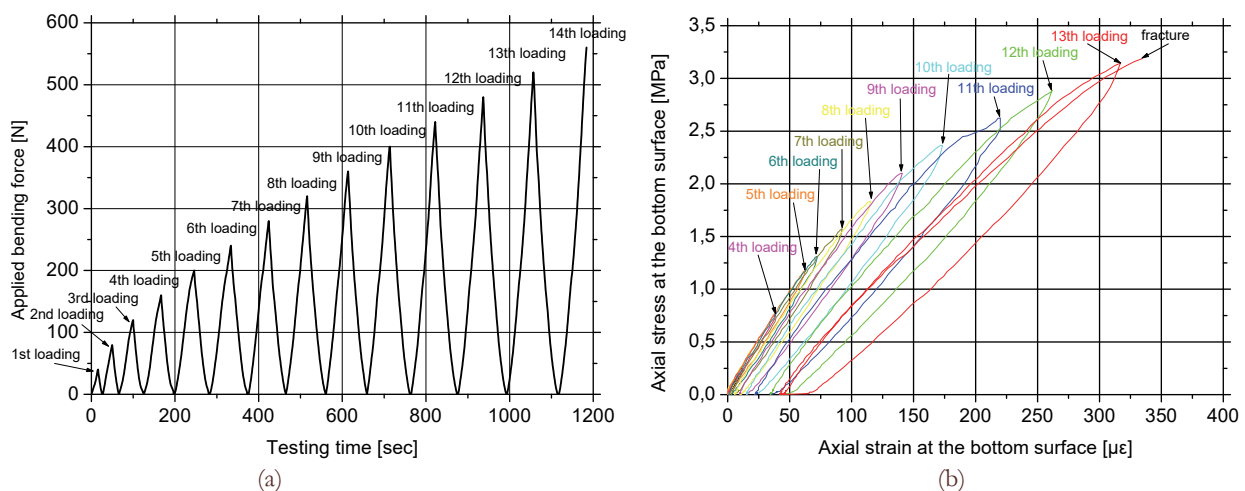

(a)

(b)

Figure 10: (a) Applied increasing loading – unloading protocol and (b) mechanical response per different loading loop under four point bending test.

Fig. 11 shows the comparison of the mechanical response from readings of the embedded FOBG (red curves) as well as form the attached surface strain gauge (black curves). For the extremely low loading values (Figs. 11a to c), actually no

discrepancies are noticed when compared the embedded sensor with the traditional, attached strain gauge. With increasing loading loop (Figs. 11d and e), higher discrepancy between the two types of sensors is observed. Similar results were noticed for the same fibers embedded in GFRP under bending loads [20]. Finally, loss in contact of transmitted light was observed in loading branch of the ninth loop (Fig. 11f) and the recording phase of FOBG was terminated after this loop.
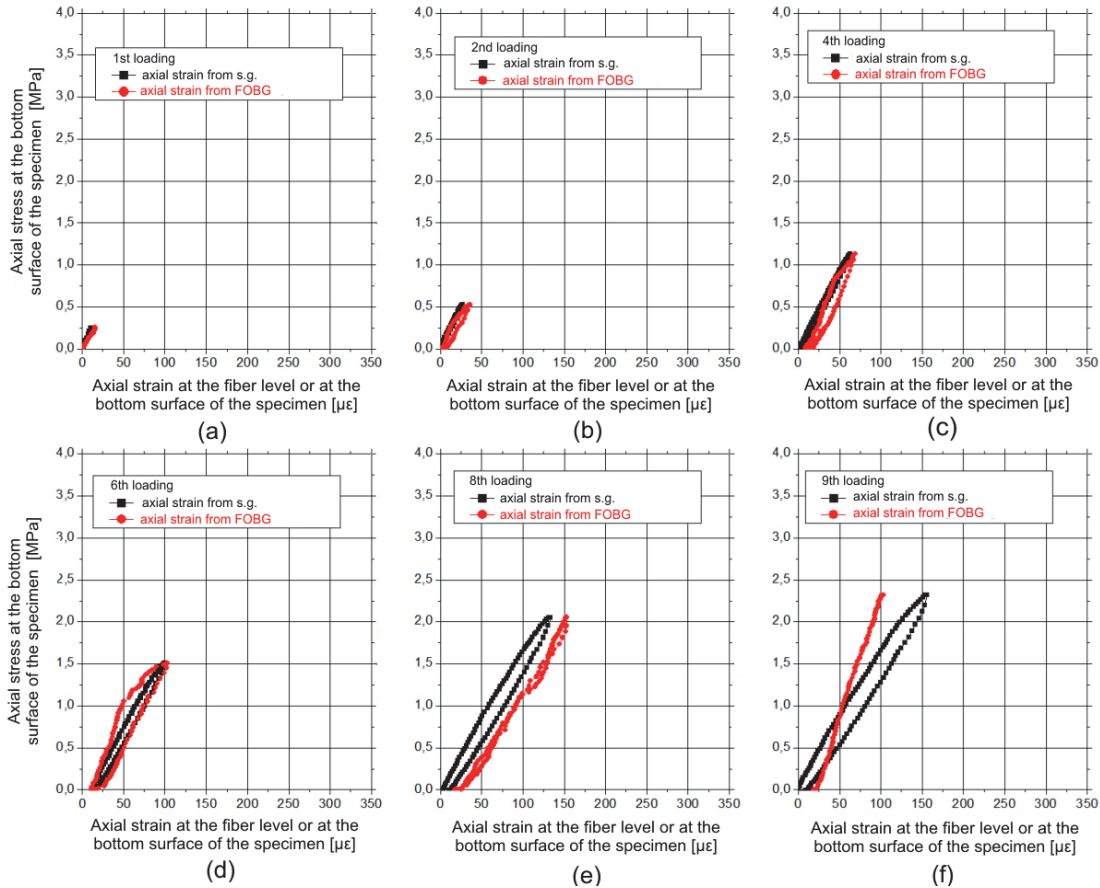

Figure 11: Increasing loading – unloading loops in type I specimen with embedded optical fiber and attached strain gauge for maximum loadings up to: (a) 40 N, (b) 80 N, (c) 160 N, (d) 240 N, (e) 320 N and (f) 360 N.

The same experimental protocol was applied on prismatic cementitious specimens with embedded coated PVA-CNT fiber as well as coated and annealed PVA-CNT fiber, where the test results can be seen in Figs. 12 and 13, respectively. For the case of the embedded coated PVA-CNT fiber, Fig. 12 shows the mechanical response (black curves) as well as the ERC response of the embedded fiber. Regarding the mechanical response of the specimen, it is evident that a linear correlation between stress–strain is observed up till maximum load up till 200 N (Figs. 12a to c). This is actually the elastic limit of the prismatic specimen under bending loads as for increasing applied load (Fig. 12d) hysteresis loop is formulated during unloading branch. Hysteresis loop is even higher noticeable at higher load (Fig. 12e) and finally fracture occurs at 520 N applied load (Fig. 12f). Hysteresis loops are evidence of inelastic mechanical response of the specimen and damage in the matrix (probably matrix cracking) of the specimen. On the contrary, the ERC readings of the embedded fiber seems not to follow the applied loading protocol, losing cohesion with the applied stress / strain variance with the very start mechanical response. This might be due to the insufficient bonding of the fiber with the surrounding matrix [21], as previously documented with the respective monotonic tests. Bonding loss of the specific interphase is probably the best answer to explain the inaccurate ERC values at high applied stress / strain levels.

Fig. 13 shows the respective results of the embedded coated and annealed PVA-CNT fiber in the prismatic specimen under the same experimental loading protocol. Similar to the previous fiber, ERC measurements trend is also noticed for this case. Linearity between stress-strain is noticed for the low applied loadings, while hysteresis loops till fracture is evident as also noticed in [20]. Regarding the ERC measurements, this type of fiber seems to be more promising as it gives not ambiguous, scattered data as noticed for the previous type of fiber. Coated and annealed PVA-CNT fiber gives a linear increase in ERC with the increased stress / strain for the low loading range; loss in coherency for higher applied

loads gives measurements that can be hardly be quantified and processed. To this end, this fiber seems to be more favorable for future research in case that proper interphase will be created with the surrounding matrix.
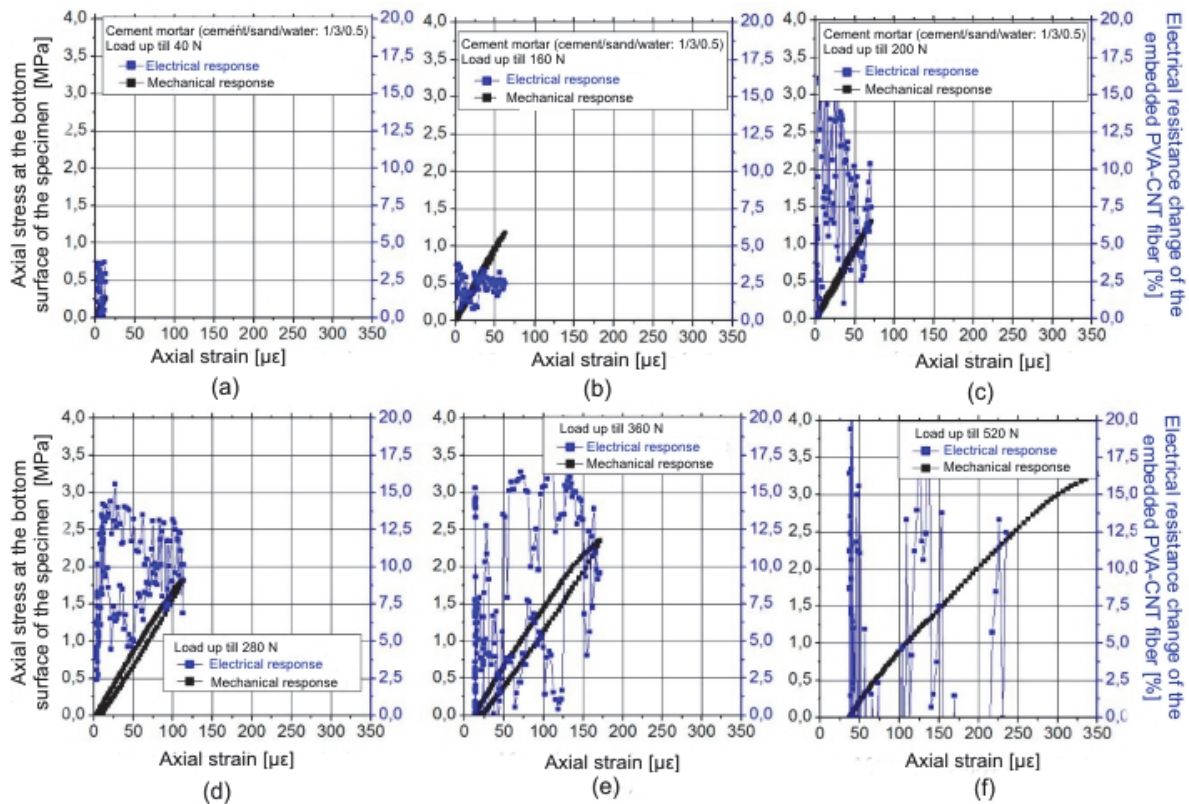

Figure 12: Incremental loading – unloading loops in type I specimen with embedded coated PVA-CNT fiber for applied loadings up till: (a) 40 N, (b) 160 N, (c) 200N, (d) 280 N, (e) 360 N and (f) 520 N (fracture).

Fig. 14 shows the respective test results for the type II specimen with the surface attached fiber. Test results are more encouraging when compared with the respective constant amplitude results, as the screening of the ERC measurements is evident. Linearity between strain and ERC measurements can be justified for low strain values, while hysteresis loops are formed when unloading the specimens, e.g. [20, 21]. Definitely this kind of fiber can be used for sensing applications, provided that optimization on the attaching procedure and loading transfer methodology should be applied.

CONCLUSIONS

- An experimental work has been performed to successfully accomplish the embedding procedure of the sensing fiber without damaging the sensor or the hosting medium.
- Monotonic bending tests with in-situ electrical resistance change of the embedded fiber showed encouraging results. Linearity between bending strain at the bottom of the specimen and electrical resistance change of the embedded fiber for the low applied loading regime was evident. For higher applied monotonic stress, a sudden drop in ERC was noticed that was attributed to the loss of the interphase between the fiber and the specimen as well as micro-cracking formation at the sequence of the test up till fracture.
- The embedded coated PVA-CNT fiber gave satisfactory results on the monotonic bending tests when compared against the coated and annealed PVA-CNT fiber. It enabled the linearity between applied strain and ERC at the low loading regime and generally gave higher ERC values when mechanically stressed that enables for the better screening of the test results.
- For the case of constant amplitude tests, the embedded coated PVA-CNT fiber gave the best results, showing a trend of continuous increasing ERC measurements that can be justified with continuously increasing damage in the

material. On the contrary, the surface attached version of the same fiber gave unsatisfactory results due to possible debonding / loss of coherency with the attaching medium.
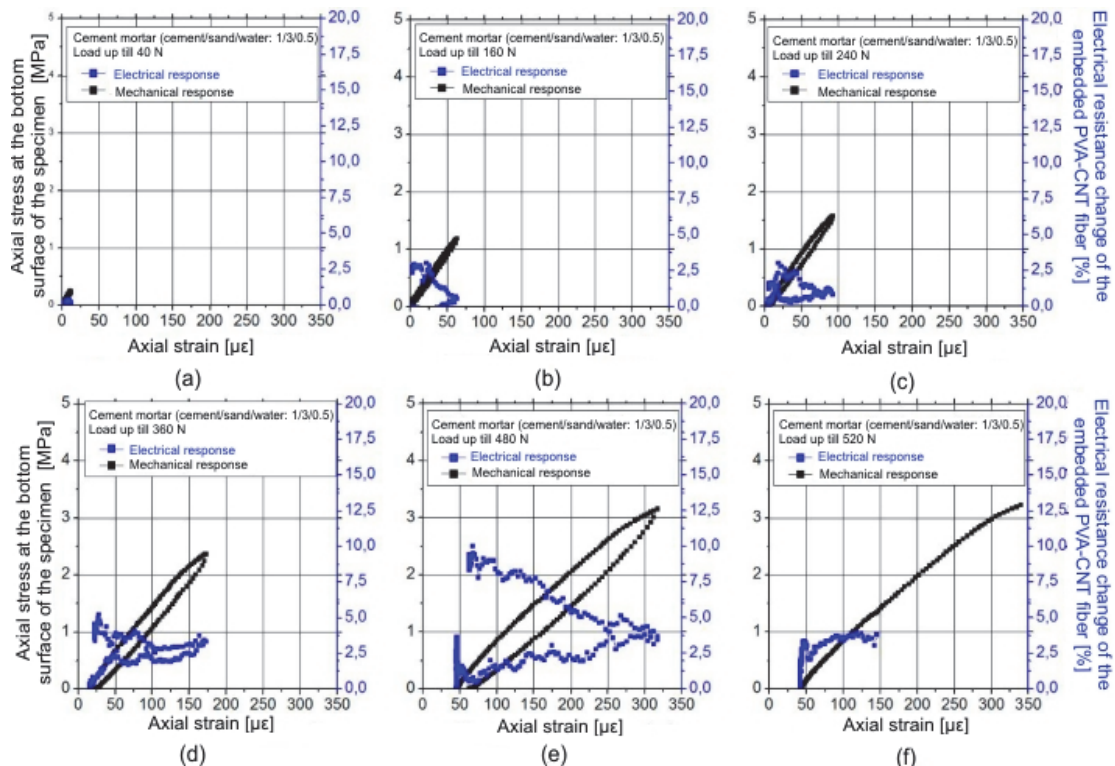

Figure 13: Incremental loading – unloading loops in type I specimen with embedded coated PVA-CNT fiber for applied loadings up till: (a) 40 N, (b) 160 N, (c) 240 N, (d) 360 N, (e) 480 N and (f) 520 N (fracture).
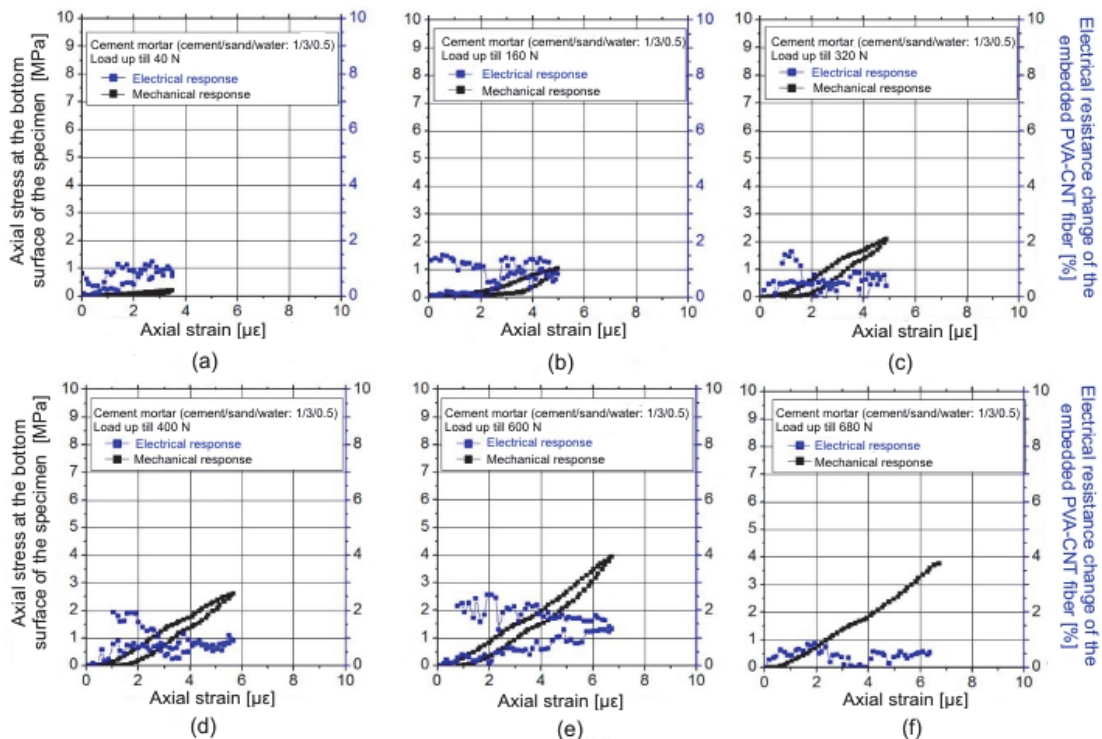

Figure 14: Incremental loading – unloading loops in type II specimen with surface-attached coated and annealed PVA-CNT fiber for applied loadings up till: (a) 40 N, (b) 160 N, (c) 320 N, (d) 400 N, (e) 600 N and (f) 680 N.

- For the case of incremental increasing loading-unloading loops, the FOBGs seems to be the more mature technology for strain sensing of cementitious material for low straining regime. For large displacements/strains damage on the brittle fiber might occur that might terminate the measurements of the sensor. The embedded coated and annealed PVA-CNT fiber gave the best sensing response in the incremental loading – unloading loops, especially at the high loading regime. Linearity between applied strain and ERC measurements was noticed for the low applied loadings while hysteresis loops were formed after every unloading branch.
- Coated and annealed PVA-CNT fiber also gave satisfactory results when surface attached at the bottom surface of the prismatic specimens, showing that annealing plays a significant role on the sensing ability of the fiber, despite lower the screening ability of the fiber itself.

ACKNOWLEDGEMENTS

REFERENCES

[1] Kourkoulis, S.K., Prassianakis, I., Agioutantis, Z., Exadaktylos, G.E., Reliability assessment of the NDT results for the internal damage of marble specimens, International Journal of Material and Product Technology, 26 (2006) 35-56.

[2] Kourkoulis, S.K., Ganniari-Papageorgiou, E., Bending of fragmented architraves restored with bolted titanium bars: A numerical analysis, Engineering Transactions, 56 (2008) 95-135.

[3] Kourkoulis, S.K., Ganniari-Papageorgiou, E., Mentzini, M., Dionysos marble under bending: A contribution towards understanding the fracture of the Parthenon architraves, Engineering Geology, 115 (2010) 246-256.

[4] Kourkoulis, S.K., Mentzini, M., Ganniari-Papageorgiou, E., Restored marble epistyles under bending: a combined experimental and numerical study, International Journal of Architectural Heritage, 7 (2013) 89-115.

[5] Kourkoulis, S.K, Ganniari-Papageorgiou, E., Restoring fragmented marble epistyles: some critical points, Journal of Cultural Heritage, 11 (2010) 420-429.

[6] Kourkoulis, S.K., Pasiou, E.D., Triantis, D., Stavrakas, I., Hloupis, G., Innovative experimental techniques in the service of restoration of stone monuments - Part I: The experimental set up, Procedia Engineering, 109 (2015) 268-275.

[7] Triantis, D., Stavrakas, I., Pasiou, E.D., Hloupis, G., Kourkoulis, S.K., Innovative experimental techniques in the service of restoration of stone monuments - Part II: Marble epistyles under shear, Procedia Engineering, 109 (2015) 276-284.

[8] Hofer, B., Fibre optic damage detection in composite structures, Composites, 18 (1987) 309-316.

[9] Waite, S.R., Tatam, R.P., Jackson, A., Use of optical fibre for damage and strain detection in composite materials, Composites, 19 (1988) 435-442.

[10] Takeda, S., Okabe, Y., Takeda, N., Delamination detection in CFRP laminates with embedded small-diameter fiber Bragg grating sensors, Composites Part A 33 (2002) 971-980.

[11] Park, J.M., Lee, S.I., Kwon, O.Y., Choi, H.S., Lee, J.H., Delamination detection in CFRP laminates with embedded small-diameter fiber Bragg grating sensors, Composites Part A 34 (2003) 203-216.

[12] Leng, J., Asundi, A., Structural health monitoring of smart composite materials by using EFPI and FBG sensors, Sensors and Actuators A: Physical, 103 (2003) 330-340.

[13] Ohtsu, M., Recommendations of RILEM Technical Committee 212-ACD: acoustic emission and related NDE techniques for crack detection and damage evaluation in concrete: 3. Test method for classification of active cracks in concrete structures by acoustic emission. Materials and Structures, 43 (2010) 1187-1189.

[14] Alver, N., Tanarslan, H.M., Sülün, Ö.Y., Ercan, E., Karcı, M., Selman, E., Ohno, K., Effect of CFRP-spacing on fracture mechanism of CFRP-strengthened reinforced concrete beam identified by AE-SiGMA, Construction and Building Materials, 67 (2014) 146-156.

[15] Mpalaskas, A.C., Vasilakos, I., Matikas, T.E., Chai, H.K., Aggelis, D.G., Monitoring of the fracture mechanisms induced by pull-out and compression in concrete, Engineering Fracture Mechanics, 128 (2014) 219-230.

[16] Sagar, R.V., Raghu Prasad, B.K., A review of recent developments in parametric based acoustic emission techniques applied to concrete structures. Nondestructive Testing and Evaluation, 27 (2012) 47-68.

[17] Vigolo, B., Penicaud, A., Coulon, C., Sauder, C., Pailler, R., Journet, C., Bernier, P., Poulin, P., Macroscopic fibers and ribbons of oriented carbon nanotubes, Science, 290 (2000) 1331-1334.

[18] Mercader, C., Denis-Lutard, V., Jestin, S., Maugey, M., Derré, A., Zakri, C., Poulin, P., Scalable process for the spinning of PVA–carbon nanotube composite fibers, Applied Polymer Science, 125 (2012) 191-196.

[19] Alexopoulos, N.D., Bartholome, C., Poulin, P., Marioli-Riga, Z., Structural health monitoring of glass fiber reinforced composites using embedded carbon nanotube (CNT) fibers, Comp. Sci. Technol., 70 (2010) 260-271.

[20] Alexopoulos, N.D., Bartholome, C., Poulin, P., Marioli-Riga, Z., Damage detection of glass fiber reinforced composites using embedded PVA–carbon nanotube (CNT) fibers, Comp. Sci. Technol., 70 (2010) 1733-1741.

[21] Alexopoulos, N.D., Jaillet, C., Zakri, C., Poulin, P., Kourkoulis, S.K., Improved strain sensing performance of glass fiber polymer composites with embedded pre-stretched polyvinyl alcohol–carbon nanotube fibers, Carbon, 59 (2013) 65-75.

[22] ASTM D305-06 Standard Practice for Mechanical Mixing of Hydraulic Cement Pastes and Mortars of Plastic Consistency, ASTM International, 100 Barr Harbor Drive, PO Box C700, West Conshohocken, United States.

[23] Nahata, Y., Kholia, N., Tank, T.G., Effect of Curing Methods on Efficiency of Curing of Cement Mortar, APCBEE Procedia, 9 (2014) 222-229.

[24] ASTM D6272 Standard Test Method for Flexural Properties of Unreinforced and Reinforced Plastics and Electrical Insulating Materials by Four-Point Bending ASTM International, 100 Barr Harbor Drive, PO Box C700, West Conshohocken, United States.